Journal of Power Sources 191 (2009) 240–252

Contents lists available at ScienceDirect

Journal of Power Sources

journal homepage: www.elsevier.com/locate/jpowsour

Percolation theory to predict effective properties of solid oxide fuel-cell composite electrodes

Daifen Chen [a], Zijing Lin [a], Huayang Zhu [b], Robert J. Kee [b,*]

[a] Hefei National Laboratory for Physical Sciences at the Microscale and Dept. of Physics, University of Science and Technology of China, Hefei 230026, PR China
[b] Engineering Division, Colorado School of Mines, Golden, CO 80401, USA

ARTICLE INFO

Article history:
Received 11 January 2009
Accepted 17 February 2009
Available online 3 March 2009

Keywords:
Percolation theory
SOFC
Effective conductivity
Effective three-phase boundary length

ABSTRACT

A micromodel based upon percolation theory is developed to predict effective properties in composite electrodes for solid oxide fuel-cell (SOFC) applications. The theory considers binary and multi-component mixtures of particles that are either ion or electron conductors. The model predicts effective ionic and electronic conductivities, three-phase boundary lengths, and hydraulic pore radii. The effective properties depend upon primary physical characteristics, including average particle-radii, volumetric packing densities, particle contact angles, and porosity. All results are presented in nondimensional form, which provides considerable generality in their practical application.

1. Introduction

composite electrodes play critical roles in most solid oxide fuel-cell (SOFC) architectures. A typical composite anode is a mixture of Ni and yttria-stabilized zirconia (YSZ). A typical composite cathode is a mixture of lanthanum-doped strontium manganate (LSM) and YSZ. It is well known that the composite-electrode architecture, including functional grading, is important to overall fuel-cell performance [1–3]. Recently, several groups have reported significantly improved performance by introducing nanoscale particles into composite electrodes [4–8]. There is certainly a need to understand quantitatively the influence of composite microstructure on fuel-cell operation. Applying that understanding is important to the design, optimization, and fabrication of certain microstructure architectures as a means to achieve high fuel-cell performance.

Composite electrodes are frequently thought of and modeled as random mixtures of spherical particles. The mixtures contain electrolyte particles (e.g., ion conducting YSZ) and electrode particles (e.g., electron conducting Ni). Composite-electrode fabrication usually begins by mixing together electrode and electrolyte particles followed by sintering at high temperature. High-resolution microscopic images of actual composite electrodes reveal that the "particles" are not spherical, even when the particles may have been initially spherical before sintering [9]. Nevertheless, models based upon random arrays of spherical particles provide important qualitative insight and quantitative design guidance.

The present paper develops and extends coordination-number and percolation theory to predict effective properties of composite electrodes. Based upon theory at the particle scale, important characteristics of the composite structure can be derived. Such effective properties (e.g., electron and ion conductivity, three-phase boundary length, and pore radius) are needed in larger scale models that consider the entire fuel-cell system [10,11]. The effective properties depend upon microstructural features, including particle-radii distributions, gas-phase porosity, particle overlap, and relative electrode and electrolyte particle loading. The composite performance also depends upon intrinsic properties (e.g., conductivity) of the particle materials. The results herein are presented in nondimensional form, affording a degree of generality.

The percolation theory in this paper builds on the foundation of significant earlier literature. As part of a more general effort to develop micromodels of SOFC systems, Costamanga et al. [12,13] developed percolation models for composite electrodes. Chan et al. [14,15] also developed SOFC micromodels that incorporate percolation-theory-based effective properties. Janardhanan et al. [16] used percolation theory to predict three-phase boundary lengths as functions of particle dimensions and packing density.

Percolation theory depends upon the concept of coordination numbers, representing the number of contacts that a certain particle makes with neighboring particles. The micromodel developed

* Corresponding author. Tel: +1 303 273 3379; fax: +1 303 273 3602.
E-mail address: rjkee@mines.edu (R.J. Kee).

0378-7753/$ – see front matter © 2009 Elsevier B.V. All rights reserved.
doi:10.1016/j.jpowsour.2009.02.051

Nomenclature

$a_{k,\ell}$	cross-sectional area per contact between a k- and an ℓ-particle (m^2)
$A^V_{ed,el}$	overall binary phase contact area per unit volume (m^{-1})
$A^V_{s,g}$	interfacial area per unit volume between the solid particles and pores (m^{-1})
ed_k	subscript for electrode particles in size class k
el_k	subscript for electrolyte particles in size class k
ed	subscript for m kinds of electrode particles
el	subscript for n kinds of electrolyte particles
$l_{k,\ell}$	contact perimeter between a k-particle and an ℓ-particle (m)
L	geometric thickness of composite electrode (m)
L^{ter}_{el}	total thickness of grain boundary along the current path (m)
M	number of particle types
m	kinds of size class for electrode particles
n^V_k	number of k-particles per unit volume
n^S_k	number of k-particles per unit electrolyte surface area
n	kinds of size class for electrolyte particles
$N_{k,\ell}$	average contact number of ℓ-particles with a k-particle in an idealized medium
P_k	percolation probability of k-particle
r_k	radii of k-particles (m)
r_c	neck radius between two connect particles (m)
r_g	hydraulic radius for gas flow (m)
$\tilde{r}_g$	nondimensional hydraulic radius
R^{ter}_{el}	ion-transport resistance (Ω)
S_ℓ	surface-area fraction of all ℓ-particles
S	geometric cross-sectional area of composite electrode (m^2)
S^{ter}_{el}	effective contact surface area between el-particles per particle layer (m^2)
x	fraction of solid surface areas belonging to the solid-pore binary phase boundary area
Z_k	average number of contacts between a k-particle and neighboring particles of all types
$Z_{k,\ell}$	average number of contacts between a k-particle and ℓ-particles
$\bar{Z}$	overall average coordination number of all solid particles
$Z_{el,el}$	average coordination number for all n electrolyte particles

Greek letters

δ	thickness of boundary between particles (m)
ϵ	relative error between $\zeta_k Z_{k,\ell}$ and $\zeta_\ell Z_{\ell,k}$
λ^V_{TPB}	TPB length per unit volume (m^2)
$\lambda^V_{TPB,eff}$	effective TPB length per unit volume (m^2)
$\tilde{\lambda}^V_{TPB,eff}$	nondimensional effective TPB length per unit volume
$\lambda^S_{TPB,eff}$	effective TPB length per unit electrolyte surface area, m^{-1}
$\tilde{\lambda}^S_{TPB,eff}$	nondimensional effective TPB length per unit electrolyte surface area
μ	Bruggeman factor
ψ_k	volume fraction of k-particles relative to the total solids
ψ^c_k	percolation threshold of k-particles
$\psi^o_{ed_k}$	relative volume fraction of k-class particles within all m electrode particles
ϕ_g	porosity
$\sigma^{tra,o}$	intrinsic material conductivity (S/m)
$\sigma^{tra,eff}$	effective intra-particle conductivity (S/m)
$\tilde{\sigma}^{tra,eff}$	nondimensional effective intra-particle conductivity
$\sigma^{ter,o}$	intrinsic conductivity of the particle interface (S/m)
$\sigma^{ter,eff}$	effective inter-particle conductivity (S/m)
$\tilde{\sigma}^{ter,eff}$	nondimensional effective inter-particle conductivity
θ	contact angle between two particles
ξ_{el}	effective relative density of electrolyte particles
ζ_k	number fraction of k-particles

by Bouvard and Lange has been widely used to estimate coordination numbers for binary systems [17]. Suzuki and Oshima developed a theory that can be used to estimate coordination numbers in multi-component mixtures [18–20].

The present paper develops some significant extensions of earlier research. The approach considers multi-component particle mixtures and satisfies the contact-number conservation requirement [12]. Based upon the underpinning functional forms, all the effective properties are represented in nondimensional form. Consequently, the results are general in the sense that they are not specific to a particular electrode structure. Rather, once physical parameters are specified, relevant effective properties can be easily extracted from the nondimensional properties.

It should be mentioned that direct simulation of large particle arrays is an alternative to percolation theory for estimating effective properties [21–25]. Additionally, such multi-particle simulations can provide quantitative information concerning the coordination numbers that appear in the percolation theory.

2. Percolation theory

Percolation probabilities represent the likelihood that particles are clustered in ways that form connected conduction pathways, which is central to the effective functioning of a composite electrode [3,13,21]. The concept of coordination numbers is central to the practical implementation of percolation theory. Broadly speaking, the coordination number represents the number of contacts a particular particle makes with its neighboring particles.

Consider a multi-component mixture of randomly packed spherical particles with M particle types (M is typically a small number). For example, in a binary mixture of Ni and YSZ particles each with a single particle radius, $M = 2$. The average number of contacts Z_k between k-type particles and neighboring particles of all types is

$$Z_k = \sum_{\ell=1}^{M} Z_{k,\ell}, \tag{1}$$

where $Z_{k,\ell}$ is the number of contacts between a k-particle and ℓ-particles. Suzuki and Oshima proposed that $Z_{k,\ell}$ is proportional to S_ℓ (the surface-area fraction of all ℓ-particles) and $N_{k,\ell}$ (the average contact number of all ℓ-particles with a k-particle in a particular idealized medium) [18,20]:

$$Z_{k,\ell} = S_\ell N_{k,\ell}. \tag{2}$$

The surface-area fractions can be estimated in terms of the particle volume fractions ψ_k as

$$S_\ell = \frac{n_\ell^V 4\pi r_\ell^2}{\sum_{k=1}^{M} n_k^V 4\pi r_k^2} = \frac{\zeta_\ell r_\ell^2}{\sum_{k=1}^{M} \zeta_k r_k^2} = \frac{\psi_\ell / r_\ell}{\sum_{k=1}^{M} \psi_k / r_k} \tag{3}$$

where r_k are the particle-radii. The volume fractions may be represented as

$$\psi_k = \frac{n_k^V 4\pi r_k^3/3}{\sum_{\ell=1}^{M} n_\ell^V 4\pi r_\ell^3/3} = \frac{n_k^V r_k^3}{\sum_{\ell=1}^{M} n_\ell^V r_\ell^3}, \tag{4}$$

where n_k^V is the number of k-particles per unit volume. The number fractions ζ_k represent the fraction of k-particles, which can be written as

$$\zeta_k = \frac{n_k^V}{\sum_{\ell=1}^{M} n_\ell^V} = \frac{\psi_k / r_k^3}{\sum_{\ell=1}^{M} \psi_\ell / r_\ell^3}. \tag{5}$$

The volume fractions ψ_k are defined relative to the total solid materials, with the gas-phase porosity ϕ_g specified independently. For example a composite electrode that is (by volume) 33% Ni, 33% YSZ, and 34% pores has $\psi_{Ni} = \psi_{YSZ} = 0.5$.

The average coordination number of all particles within an M-component packed bed can be expressed as

$$\bar{Z} = \sum_{k=1}^{M} \zeta_k Z_k, \tag{6}$$

where Z_k represents the average contact number between k-type-particles and all neighboring particles (Eq. (1)).

The variable $N_{k,\ell}$ (Eq. (2)) is particular to a certain idealized two-component particle mixture (k and ℓ particles) [18]. This idealization rests upon two assumptions. First, the mixture is assumed to be dominated by ℓ particles with very few k-particles. In other words, ζ_k (the fraction of k-particles) is nearly zero and ζ_ℓ (the fraction of ℓ particles) is nearly unity. Second, the overall average coordination number within the idealized medium is the same as it is within an M-component mixture. With these assumptions, $N_{k,\ell}$ is a function of only $\bar{Z}$ and the ratio of the particle-radii. In the case that all particles are the same (i.e., $k = \ell$), the relationship between $N_{k,\ell}$ and $\bar{Z}$ is

$$N_{k,k} = \bar{Z} \tag{7}$$

Combining Eqs. (2)(3) and (7), the coordination number among the same kind of particles $Z_{k,k}$ is a function of the volume fraction and particle-radii as

$$Z_{k,k} = \bar{Z} \frac{\psi_k / r_k}{\sum_{\ell}^{M} \psi_\ell / r_\ell}. \tag{8}$$

This expression leads to a good estimate in binary particle mixtures of the relationship between the percolation threshold for same-type particles (i.e., percolation threshold for k or ℓ particles) and the particle-size ratio (i.e., r_k/r_ℓ) [12,26].

In cases where $k \neq \ell$, the relationship between the $N_{k,\ell}$ and $\bar{Z}$ is more complicated than is indicated by Eq. (7). Suzuki and Oshina proposed that $N_{k,\ell}$ can be estimated as [18],

$$N_{k,\ell} = \frac{0.5(2-\sqrt{3}) N_{k,k} (r_k/r_\ell + 1)}{1 + r_k/r_\ell - (r_k/r_\ell (r_k/r_\ell + 2))^{1/2}}. \tag{9}$$

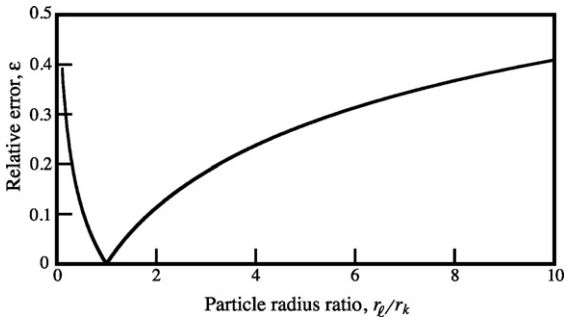

Fig. 1. Relative error in contact conservation associated with applying Eq. (9) in a multi-component particle mixture.

However, this expression does not satisfy the necessary contact-number conservation principle (i.e., $\zeta_k Z_{k,\ell} = \zeta_\ell Z_{\ell,k}$). Contact-number conservation means that the net contact between the k-particles and ℓ-particles must be equal to the contact between ℓ-particles and k-particles [12]. The relative difference between $\zeta_k Z_{k,\ell}$ and $\zeta_\ell Z_{\ell,k}$ when using Eq. (9) can be evaluated as

$$\epsilon = \frac{|\zeta_k Z_{k,\ell} - \zeta_\ell Z_{\ell,k}|}{\min(\zeta_k Z_{k,\ell}, \zeta_\ell Z_{\ell,k})} \tag{10}$$

This relative error is a function of the particle-radii ratio (r_ℓ/r_k), but is independent of the average coordination number $\bar{Z}$ and the number of components M in the mixture. As illustrated in Fig. 1, the relative error increases greatly as the particle sizes vary. Thus, an alternative approach is needed to determine $N_{k,\ell}$.

Beginning with some fundamental principles of percolation theory, an alternative approach is taken for evaluating $N_{k,\ell}$. For a binary mixture, the following set of equations must hold:

$$Z_k = Z_{k,k} + Z_{k,\ell}, \quad Z_\ell = Z_{\ell,\ell} + Z_{\ell,k}, \tag{11}$$

$$\bar{Z} = \zeta_k Z_k + \zeta_\ell Z_\ell, \tag{12}$$

$$\zeta_k Z_{k,\ell} = \zeta_\ell Z_{\ell,k}, \tag{13}$$

$$\zeta_k + \zeta_\ell = 1, \tag{14}$$

$$Z_{k,k} = N_{k,k} \frac{\zeta_k r_k^2}{\zeta_k r_k^2 + \zeta_\ell r_\ell^2}, \quad Z_{\ell,\ell} = N_{\ell,\ell} \frac{\zeta_\ell r_\ell^2}{\zeta_k r_k^2 + \zeta_\ell r_\ell^2}, \tag{15}$$

$$Z_{k,\ell} = S_\ell N_{k,\ell} \tag{16}$$

Substituting Eqs. (11) and (13) into Eq. (12), the average coordination number can be written as

$$\bar{Z} = \zeta_k Z_{k,k} + \zeta_\ell Z_{\ell,\ell} + 2\zeta_k Z_{k,\ell}. \tag{17}$$

The coordination number $Z_{k,\ell}$ can be determined by substituting Eq. (15) into Eq. (17), yielding

$$Z_{k,\ell} = \frac{\bar{Z}}{2\zeta_k} \left(1 - \frac{\zeta_k^2 r_k^2 + \zeta_\ell^2 r_\ell^2}{\zeta_k r_k^2 + \zeta_\ell r_\ell^2} \right) = 0.5(1 + r_k^2/r_\ell^2) S_\ell \bar{Z} \tag{18}$$

By comparing Eq. (18) with Eq. (16), it is evident that

$$N_{k,\ell} = 0.5(1 + r_k^2/r_\ell^2)\bar{Z}. \tag{19}$$

Eq. (19) is equally applicable for $k = \ell$ and $k \neq \ell$. It is clear that $N_{k,\ell}$ is a function of only $\bar{Z}$ and the radii of the k- and ℓ-particles. Consequently, Eq. (19) can be used to evaluate the coordination number between two particle types in a multi-component mixture.

Using Eq. (4), Eq. (18) can be rewritten in terms of the particle volume fractions ψ_k as

$$Z_{k,\ell} = 0.5(1 + r_k^2/r_\ell^2)\bar{Z} \frac{\psi_\ell / r_\ell}{\sum_{k=1}^{M} \psi_k / r_k}. \tag{20}$$

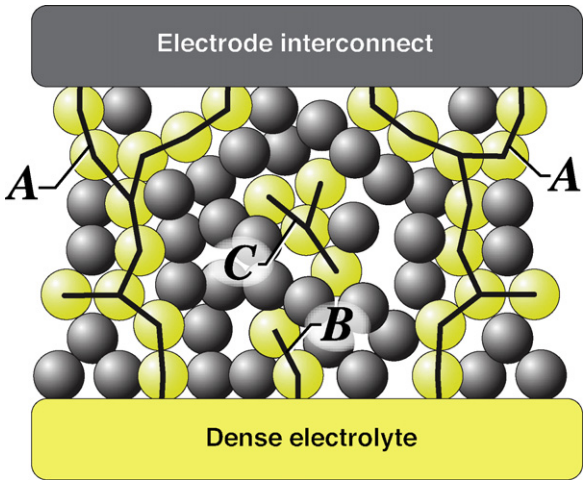

Fig. 2. Conceptual illustration of a composite SOFC electrode. The dark particles represent the electrode particles and the light particles represent the electrolyte.

The coordination number for the k-particles can be obtained by substituting Eqs. (8) and (20) into Eq. (1), yielding

$$Z_k = \sum_{\ell=1}^{M} Z_{k,\ell} = \frac{\bar{Z}}{2}\left(1 + \frac{r_k^2}{\sum_{\ell=1}^{M}\zeta_\ell r_\ell^2}\right). \tag{21}$$

The validity of the alternative model proposed above is supported by comparison with an expression proposed by Bouvard and Lange [17]. Considering a binary mixture with an overall coordination number $\bar{Z} = 6$, Eq. (21) yields

$$Z_k = 3 + \frac{3r_k^2}{\zeta_k r_k^2 + \zeta_\ell r_\ell^2}. \tag{22}$$

This result is the same as that reported by Bouvard and Lange [17]. Further validation, as discussed below, is achieved by comparing with the computational simulated results for binary mixtures as reported by Suzuki and Oshima [18].

3. Binary mixture properties

Initially consider applying the percolation theory to a two-component SOFC porous composite electrode that is composed of ionic and electronic-conducting particles (labeled "el" for electrolyte such as YSZ and "ed" for electrode such as Ni).[1]

3.1. Percolation probabilities

Fig. 2 illustrates a two-component randomly packed mixture of the spherical particles, where three different cluster types are represented for the electrolyte particles. Following the nomenclature of Costamanga, et al. [12], such clusters may be characterized as

A clusters: The electrolyte particles form a percolated cluster that extends through the entire thickness of the composite electrode (i.e., from the dense electrolyte to the electrode current collector).
B clusters: The electrolyte particles form a short network that is connected only to the dense electrolyte. Such clusters can carry ionic current into the composite-electrode structure, assuming that there is sufficient connectivity within the electrode particles to carry electronic current and thus facilitate charge-transfer reactions.
C clusters: The electrolyte particles form a completely isolated cluster. These clusters are essentially ineffective in supporting charge-transfer or current conduction.

The probability that electrolyte particles belong to an A-cluster is defined as the percolation probability of the electrolyte particle. The percolation probability can be estimated as [12]

$$P_{\mathrm{el}} = \left[1 - \left(\frac{3.764 - Z_{\mathrm{el,el}}}{2}\right)^{2.5}\right]^{0.4} \tag{23}$$

As can be seen from Eq. (8), the percolation probability depends upon the particle volume fraction, the particle-radii, and the average coordination number $\bar{Z}$. There is a threshold in the volume concentration of the electrolyte particles $\psi_{\mathrm{el}}^{\mathrm{c}}$, called the percolation threshold, below which the particles form only B and C clusters. For volume fractions above the threshold, networks of A clusters are formed. Above the percolation threshold, the composite electrode still contains a few B and C clusters. However, Costamagna shows that above the threshold most of the particles belong to A clusters [12].

Combining Eqs. (8) and (23) shows that the percolation thresholds for electrode and electrolyte particles may be represented in terms of the threshold volume fractions ($\psi_{\mathrm{ed}}^{\mathrm{c}}$ and $\psi_{\mathrm{el}}^{\mathrm{c}}$) and the ratio of particle-radii ($r_{\mathrm{el}}/r_{\mathrm{ed}}$) as

$$Z_{\mathrm{ed,ed}} = \bar{Z}\frac{\psi_{\mathrm{ed}}^{\mathrm{c}}/r_{\mathrm{ed}}}{\psi_{\mathrm{ed}}^{\mathrm{c}}/r_{\mathrm{ed}} + \psi_{\mathrm{el}}/r_{\mathrm{el}}} = 1.764 \tag{24}$$

$$Z_{\mathrm{el,el}} = \bar{Z}\frac{\psi_{\mathrm{el}}^{\mathrm{c}}/r_{\mathrm{el}}}{\psi_{\mathrm{ed}}/r_{\mathrm{ed}} + \psi_{\mathrm{el}}^{\mathrm{c}}/r_{\mathrm{el}}} = 1.764 \tag{25}$$

These relationships assist in identifying parameters that are important for predicting the performance of composite electrodes. For example, if the particle-radii are fixed, then the volume loading fractions should be established such that

$$\psi_{\mathrm{ed}}^{\mathrm{c}} < \psi_{\mathrm{ed}} < (1 - \psi_{\mathrm{el}}^{\mathrm{c}}). \tag{26}$$

By satisfying this constraint both the electrode and electrolyte particles should connect (i.e., percolate) through the entire thickness of the composite electrode.

3.2. Effective three-phase boundary length

The contact perimeter between overlapping electrode and electrolyte particles can be evaluated as $l_{k,\ell} = 2\pi r_{\mathrm{c}}$, where r_{c} is the neck radius (Fig. 3). The neck radius depends upon the smaller-particle radius and the contact angle θ as [12]

$$r_{\mathrm{c}} = \min(r_k, r_\ell)\sin\theta \tag{27}$$

When the intersection between electrode and electrolyte particles is exposed to reactive gases within pores, the exposed length of the intersection is the three-phase-boundary (TPB) length. Here the entire intersection length is assumed to be TPB length.

The TPB length per unit volume $\lambda_{\mathrm{TPB}}^{\mathrm{V}}$ of a composite electrode with a binary mixture is assumed to be the product of the contact perimeter between electrode and electrolyte particles and the number of contact points per unit volume, which is the product of

[1] Throughout this paper the word "electrode" has two different, but commonly used, meanings. On one hand, electron-conducing particles are called electrode particles. On the other hand, the entire composite structure is called the electrode. In context, the meanings are clear.

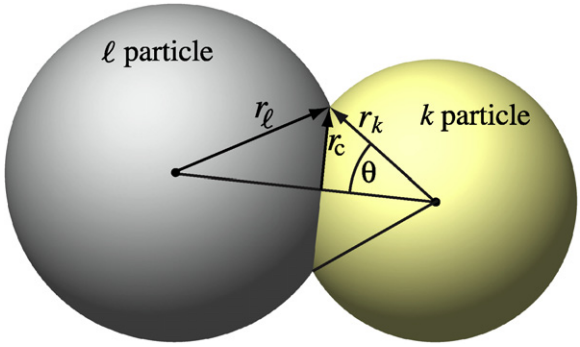

Fig. 3. Overlapping k- and ℓ-particles, forming a three-phase boundary around the intersection.

the particle number per unit volume and the coordination number [12]. That is

$$\lambda^{V}_{TPB} = l_{ed,el} n^{V}_{ed} Z_{ed,el} = l_{ed,el} n^{V}_{el} Z_{el,ed}, \quad (28)$$

where the number of k particles per unit volume within the entire composite-electrode structure can be estimated as [3,12,18]

$$n^{V}_{k} = \frac{(1-\phi_g)\psi_k}{4\pi r_k^3/3}. \quad (29)$$

The porosity (i.e., gas-phase volume fraction) is represented as ϕ_g. Generally speaking, electrodes are designed to have large TPB length. However, TPB length is only effective electrochemically if the participating particles are percolated through the thickness of electrode structure over which charge-transfer chemistry proceeds. For typical SOFC electrodes, this charge-transfer length is typically a few tens of microns [11].

To illustrate the effects of relative particle loading, Fig. 4 shows three different electrode-particle-loading scenarios as explained below:

(a) Low electrode-particle loading: Low electrode-particle loading occurs when $0 < \psi_{ed} < \psi^{c}_{ed}$. As illustrated in Fig 4 a, most of the electrolyte particles are in A-type clusters, with relatively few in B- or C-type clusters. In this case, the effective TPB regions (noted with the bracket on the left) are found only near the electrode-interconnect surface. These TPBs are potentially electrochemically active. However, the practical electrochemical activity depends upon the ability of ions to be transported from the dense electrolyte to the TPBs. This, in turn, depends upon the thickness of the composite electrode and the ion conductivity of the electrolyte particles. For very thin composite structures, where ions can propagate through the entire electrode with relatively low potential losses, most of the TPB lengths in Fig 4 a are electrochemically active. Such behavior is observed experimentally, where the polarization resistance does not depend strongly upon the composite-electrode loading fractions of electrode and electrolyte particles [12,27]. For relatively thick composite electrodes, ions cannot propagate significant distances from the dense-electrolyte surface because of low ion conductivity and thus large ohmic losses. In this case, the TPB lengths near the electrode current collector are essentially ineffective, rendering the entire composite electrode to be ineffective. Again, this behavior is observed experimentally. In relatively thick composite electrodes, polarization resistance increases sharply when the electrode particles are not fully percolated (i.e., connected networks through entire structure) [12,28,29]. Generally speaking, the ohmic resistance (ohmic overpotential) is high in composite electrodes that use electrolyte materials with relatively low ion conductivity or do not have fully percolated electrode particles.

(b) Equivalent particle loading Equivalent particle loading occurs when $\psi^{c}_{ed} < \phi_{ed} < (1-\psi^{c}_{el})$. As shown in Fig. 4 b, most of the electrode and electrolyte particles are found in A-type clusters [12]. The TPBs are distributed throughout the entire composite-electrode structure. Electrochemical charge transfer can proceed via ample TPBs near the electrolyte surface. Although there is available TPB throughout the electrode structure, the charge-transfer

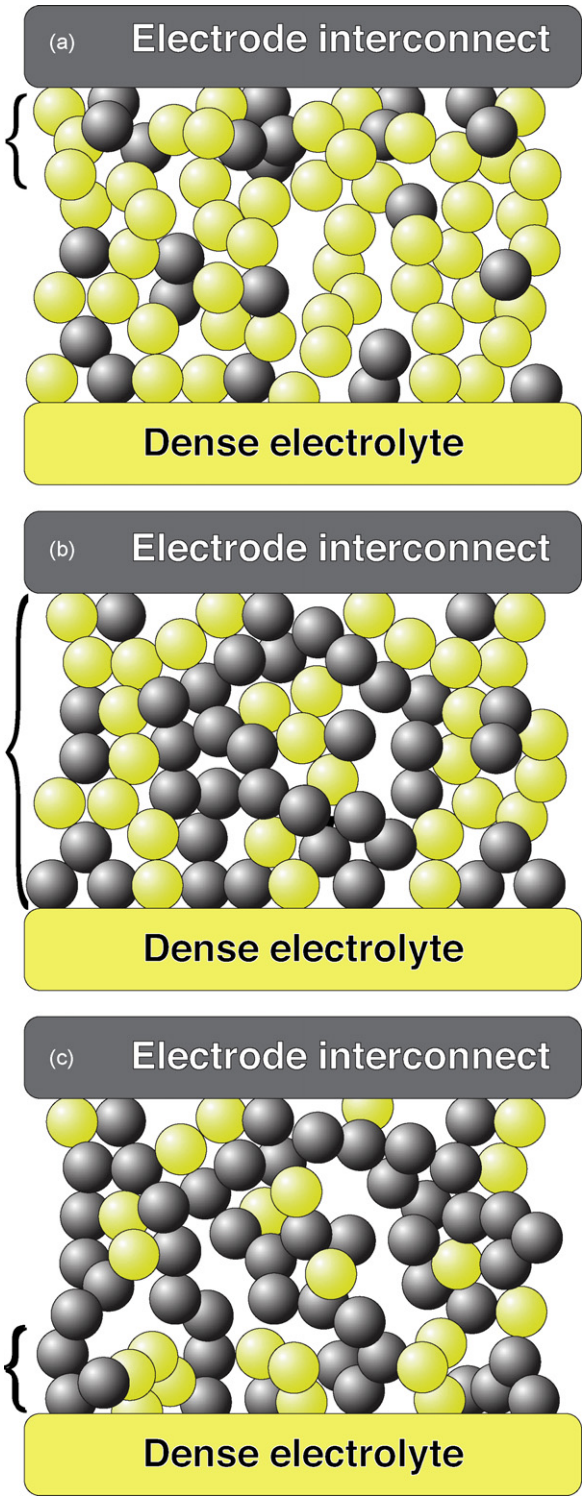

Fig. 4. Illustration of composite-electrode structures for three different loadings of electrode (dark) and electrolyte (light) particles: (a) low electrode-particle loading, $0 < \psi_{ed} < \psi^{c}_{ed}$. (b) Equivalent electrode- and electrolyte-particle loading, $\psi^{c}_{ed} < \psi_{ed} < (1-\psi^{c}_{el})$. (c) High electrode-particle loading, $(1-\psi^{c}_{el}) < \psi_{ed} < 1$.

region is usually concentrated near the dense electrolyte (typically tens of microns). Because of relatively low ion conductivity in the electrolyte particles (e.g., YSZ), the available charge is transferred from O^{2-} within the YSZ to electrons in the conduction band of the electrode particles (e.g., Ni) over a relatively short distance (i.e., the electrochemically active zone). Beyond the electrochemically active zone, the electrolyte particle clustering is unimportant. However, it is important the electrode particles percolate fully to carry electric current up to the electrode interconnect. The results in this paper are concerned primarily with composite electrodes having equivalent particle loading.

(c) High electrode particle loading: High electrode-particle loading occurs when $(1-\psi_{el}^{c}) < \phi_{ed} < 1$. As the electrode-particle loading increases (Fig. 4c), most electrode-particles belong to A-type clusters, with the electrolyte particles being dominantly in B- and C-type clusters. In this situation, the effective TPBs are concentrated near the dense-electrolyte surface. This situation could be acceptable in an SOFC anode. The charge transfer proceeds in the electrochemically active zone near the dense electrolyte, and the electronic current is easily conducted upward toward the anode interconnect. However, high electrode-particle loading may come at the expense of too few electrolyte particles and consequently too small TPB length. Such a structure would cause high activation overpotentials.

The *effective* TPB length per unit volume, which is needed to facilitate electrochemical charge transfer, depends upon the geometric TPB length (i.e., independent of cluster type) and the percolation probabilities of the electrode and electrolyte particles. The effective TPB length per unit volume can be written as

$$\lambda_{TPB,eff}^{V} = \lambda_{TPB}^{V} P_{ed} P_{el}. \tag{30}$$

3.3. Contact area

The overall contact area per unit volume $A_{ed,el}^{V}$ is assumed to be proportional to the cross-sectional area per contact between electrode and electrolyte particles and the number of contact points per unit volume. That is,

$$A_{ed,el}^{V} = a_{ed,el} n_{ed}^{V} Z_{ed,el}, \tag{31}$$

where $a_{k,\ell} = \pi r_c^2$ is the cross-sectional contact area between a k-particle and a ℓ-particle (Fig. 3).

3.4. Effective TPB length per electrolyte surface area

Electrochemical charge transfer primarily takes place at three-phase boundaries that are distributed within the electrochemically active zone near the dense electrolyte. However, there is also charge transfer at the interface between the dense-electrolyte surface and intersecting electrode particles [3]. The effective TPB length per unit electrolyte surface area is assumed to be proportional to the contact perimeter between an electrode particle and the electrolyte surface. This TPB length may be expressed as the product of the number of contact points per unit electrolyte surface area and the percolation probability of the electrode particle

$$\lambda_{TPB,eff}^{S} = l_{ed,ele} n_{ed}^{S} P_{ed}. \tag{32}$$

In this expression, "ele" represents the dense electrolyte surface, and $l_{k,ele} = 2\pi r_k \sin\theta$ is the contact perimeter between a k particle and the electrolyte surface. The number of k particles per unit electrolyte surface area can be estimated as [3]

$$n_k^{S} = \frac{(1-\phi_g)\psi_k}{2\pi r_k^2/3}. \tag{33}$$

3.5. Electronic and ionic conductivity

It is generally understood that there are important relationships among the effective electric conductivity of the composite electrode and the electrode's microstructure, including composition, porosity, particle-size ratio, etc. The effective conductivity through the electrode can be separated into intra-particle conductivity and inter-particle contributions [14,15]. The net conductivity is determined as the result of effective resistances adding in series.

3.5.1. Effective intra-particle conductivity

Chen et al. report that the effective intra-particle ionic conductivity $\sigma^{tra,eff}$ (i.e., conductivity within particles) is primarily determined by the effective relative density of electrolyte particles ξ_{el} [15]. Furthermore Jeon et al. report that intra-particle conductivity can be estimated as [3]

$$\frac{\sigma_{el}^{tra,eff}}{\sigma_{el}^{tra,o}} = \xi_{el}^{\mu} = [(1-\phi_g)\psi_{el}P_{el}]^{\mu} \tag{34}$$

where $\sigma_{el}^{tra,eff}$ is the effective intra-particle conductivity based on the geometric dimensions and $\sigma_{el}^{tra,o}$ is the intrinsic material conductivity. The Bruggeman factor μ is used to include the effects of tortuous conduction paths (μ is typically about 1.5). An expression analogous to Eq. (34) is obtained for the electronic conductivity through the electrode particles.

3.5.2. Effective inter-particle conductivity

The properties at particle interfaces (or grain boundaries) can play an important role on overall conductivity. Especially at intermediate and low temperatures, relatively low conductivity of ceramic ion conductors (e.g., YSZ) can be attributed to low conductivity at particle interfaces [15,30]. Several factors, including particle size, inter-particle area, doping level, and inter-particle material thickness, can significantly affect inter-particle conductivity. According to Chen et al. [14], the ion-transport resistance can be expressed in terms of the effective inter-particle conductivity $\sigma_{el}^{ter,eff}$ and the intrinsic conductivity of the particle interface $\sigma_{el}^{ter,o}$,

$$R_{el}^{ter} = \frac{L}{\sigma_{el}^{ter,eff} S} = \frac{L_{el}^{ter}}{\sigma_{el}^{ter,o} S_{el}^{ter}}. \tag{35}$$

In this expression S and L represent the geometric cross-sectional area and thickness of the composite electrode. L_{el}^{ter} is the total thickness of the particle interfaces along the current–conduction path. Assuming that a composite-electrode can be represented schematically as in Fig. 2, it is reasonable to assume that structure is composed of particle layers. In this case, the net length of the interface material is the product of the number of layers and the thickness of an individual particle interface δ.

The inter-particle conductivity can be evaluated as

$$\frac{\sigma_{el}^{ter,eff}}{\sigma_{el}^{ter,o}} = \frac{2r_{el}S_{el}^{ter}}{\delta S}, \tag{36}$$

where S_{el}^{ter} is the effective contact surface area between electrolyte particles per particle layer,

$$S_{el}^{ter} = a_{el,el}(2r_{el}S) n_{el}^{V} \frac{Z_{el,el}}{2} P_{el} \tag{37}$$

In other words, S_{el}^{ter} is proportional to the surface area per contact between two electrolyte particles $a_{el,el}$, the number of the electrolyte particles within a particle layer $(2r_{el}S)n_{el}^{V}$, the coordination number $Z_{el,el}$, and the percolation probability of the electrolyte particles.

For the ceramic materials, especially for the semiconducting materials, the inter-particle conductivity can significantly influence

the overall conductivity. However, for the electron-conducting metals the resistance caused by the inter-particle is usually negligibly small.

3.6. Mean hydraulic pore radius

The hydraulic radius is used commonly for describing flow in non-circular tubes and channels. Using a hydraulic radius enables flow in non-circular channels to be analyzed analogously with relatively simpler circular channels. The average pore radius is also an essential parameter in modeling multi-component porous-media gas-transport using a Dusty-Gas model [11,10].

The hydraulic radius for gas flow within a porous electrode can be written as

$$r_g = \frac{2\phi_g}{A^V_{s,g}}, \tag{38}$$

where $A^V_{s,g}$ is the interfacial area per unit volume between the solid particles and pores. The interfacial area can be estimated as

$$A^V_{s,g} = x4\pi(n^V_{ed} r^2_{ed} + n^V_{el} r^2_{el}) \tag{39}$$

where x is an adjustable factor that represents the fraction of solid surface areas belonging to the solid-pore binary phase boundary areas. It is usually reasonable to assume that factor x is the porosity ϕ_g. Using Eqs. (38) and (39) the hydraulic pore radius may be written as

$$r_g = \frac{2}{3}\left(\frac{1}{1-\phi_g}\right)\left(\frac{1}{\psi_{ed}/r_{ed} + \psi_{el}/r_{el}}\right). \tag{40}$$

4. Multi-component mixture properties

Percolation theory for multi-component mixtures is more complex than it is for binary mixtures. This is especially the case when there is a distribution of particle-sizes. Fig. 5 illustrates a composite electrode with a single electrode particle size and two sizes of electrolyte particles (designated el_1 and el_2). All the effective properties of the composite structure depend upon the particle-size distribution. The percolation probability depends upon the coordination numbers among the similar particle types (i.e., Z_{el_1,el_1}, Z_{el_2,el_2}) and also the mutual coordination numbers (i.e., Z_{el_1,el_2} and Z_{el_2,el_1}).

Consider a composite electrode that includes m particle sizes for electronic conductive material (designated $ed_1, ed_2 \cdots ed_m$) and n particle sizes for electrolyte material (designated $el_1, el_2 \cdots el_n$).

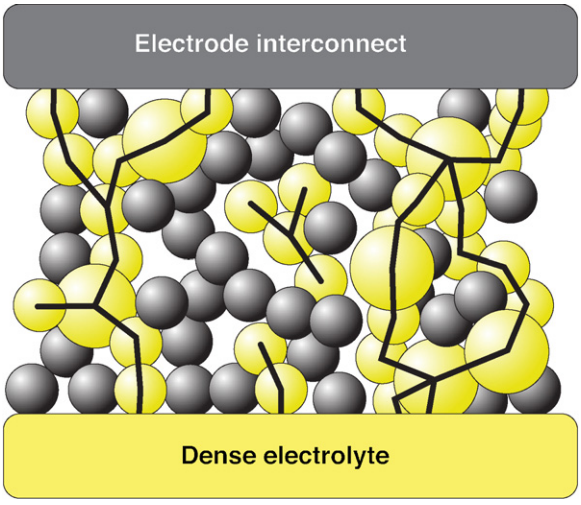

Fig. 5. Illustration of a composite electrode with two different electrolyte particle sizes.

For such a mixture, the total volume fractions of electrode and electrolyte particles may be evaluated as

$$\psi_{ed} = \sum_{k=1}^{m} \psi_{ed_k} \quad \psi_{el} = \sum_{k=1}^{n} \psi_{el_k}. \tag{41}$$

The relative volume fractions of particle sizes within the electrode and electrolyte materials are represented as

$$\psi^o_{ed_k} = \frac{\psi_{ed_k}}{\psi_{ed}}, \quad \psi^o_{el_k} = \frac{\psi_{el_k}}{\psi_{el}}. \tag{42}$$

The average coordination number for all n electrolyte particles is proposed to be

$$Z_{el,el} = \frac{\sum_{k=1}^{n}\sum_{\ell=1}^{n} \zeta_{el_k} Z_{el_k,el_\ell}}{\sum_{k=1}^{n} \zeta_{el_k}}, \tag{43}$$

where ζ_{el_k} is the number fraction of el_k particles. The percolation probability P_{el} for electrolyte particles is determined by the coordination numbers among the same kinds of particles Z_{el_k,el_k} and by the mutual coordination numbers $Z_{el_k,el_\ell}, (k \neq \ell)$. Substituting Eq. (43) into Eq. (23) yields the percolation probability P_{el}.

As in the binary situation, there is also a threshold coordination number for the electrode and electrolyte particles, $Z_{ed,ed}$ and $Z_{el,el}$, respectively. Above the threshold the particles are connected through the entire composite-electrode thickness [12].

$$Z_{ed,ed} = 1.764, \quad Z_{el,el} = 1.764 \tag{44}$$

Variables contributing to the percolation threshold are the radii ratios and particle volume fractions $\psi^o_{ed_k}(k \in m)$, $\psi^o_{el_\ell}(\ell \in n)$ and ψ_{ed}. Assuming that the radii ratios among all particle types and all volume fractions corresponding to the materials ($\psi^o_{ed_k}$ and $\psi^o_{el_k}$) are fixed, thresholds in the total volume fractions of electrode and electrolyte particles (ψ^c_{ed} and ψ^c_{el}) can be determined. Above these thresholds electrode and electrolyte materials are connected through the composite-electrode structure.

The effective per unit volume TPB lengths can be evaluated as

$$\lambda^V_{TPB,eff} = \sum_{k=1}^{m}\sum_{\ell=1}^{n} l_{ed_k,el_\ell} n^V_{ed_k} Z_{ed_k,el_\ell} P_{ed} P_{el}, \tag{45}$$

where $n^V_{ed_k}$ is the number per unit volume of electrode particles in size class k. The contact perimeter between overlapping electrode (ed_k) and electrolyte particles (el_ℓ) $l_{ed_k,el_\ell} = 2\pi r_c$ is evaluated as in the binary case, but now accommodating a range of particle sizes (Fig. 3).

The effective TPB lengths per unit electrolyte surface area can be estimated as

$$\lambda^S_{TPB,eff} = \sum_{k=1}^{m} l_{ed_k,ele} n^S_{ed_k} P_{ed}, \tag{46}$$

where $n^S_{ed_k}$ is the number per unit surface area of electrode particles in size class k.

The effective intra-particle ion conductivity can be estimated as

$$\frac{\sigma^{tra,eff}_{el}}{\sigma^{tra,o}_{el}} = \xi^{\mu}_{el} = \left[\sum_{k=1}^{n} (1-\phi_g)\psi_{el_k} P_{el}\right]^{\mu}. \tag{47}$$

This expression is analogous to Eq. (34) for the binary situation.

The effective conduction contact areas between el_k particles and neighboring electrolyte particles can be estimated as

$$S^{\mathrm{ter}}_{\mathrm{el}_k} = \sum_{\ell=1}^{n} a_{\mathrm{el}_k,\mathrm{el}_\ell}(r_{\mathrm{el}_k}S)n^{\mathrm{V}}_{\mathrm{el}_k}Z_{\mathrm{el}_k,\mathrm{el}_\ell}P_{\mathrm{el}} \tag{48}$$

The effective inter-particle ionic conductivity can be estimated as

$$\sigma^{\mathrm{ter,eff}}_{\mathrm{el}} = \sigma^{\mathrm{ter,o}}_{\mathrm{el}} \frac{\sum_{k=1}^{n} 2r_{\mathrm{el}_k}S_{\mathrm{el}_k}}{\delta S}. \tag{49}$$

The mean hydraulic radius in multi-component mixture may be estimated as

$$r_{\mathrm{g}} = \frac{2}{3}\left(\frac{1}{1-\phi_{\mathrm{g}}}\right)\left(\frac{1}{\sum_{k=1}^{m}\psi_{\mathrm{ed}_k}/r_{\mathrm{ed}_k} + \sum_{\ell=1}^{n}\psi_{\mathrm{el}_\ell}/r_{\mathrm{el}_\ell}}\right). \tag{50}$$

5. Results and discussion

5.1. Model validation

It is generally difficult to measure the coordination number in either binary or multi-component mixtures. Simulations of random arrays of particles are usually used to establish coordination numbers for particular packing scenarios. Fig. 6 shows electrode and electrolyte coordination numbers in binary mixtures as functions of the fractional loading of electrode particles. In all cases, $\bar{Z} = 6$. Four different electrolyte-electrode particle-radii ratios are considered, ranging from 1.5 to 4. Fig. 6 shows very good agreement between the percolation model and computations reported by Suzuki and Oshima [18].

For any particular composite-electrode structure $\bar{Z}$ depends upon details of the fabrication processes. Without further knowledge (experimental- or model-based) for a particular structure, it is widely assumed that $\bar{Z} = 6$ [12,14,31,32]. As discussed by Ali et al. [24], a model composite electrode may be synthesized by first assuming a random packing of spheres followed by sphere growth that simulates sintering. The random packing should lead to $\bar{Z} \approx 6$, and moderate particle growth should affect the overall coordination number only weakly. The graphical results discussed in subsequent sections of the present paper are based upon assuming that $\bar{Z} = 6$.

Because the model is analytic it can easily accept different values for $\bar{Z}$. Indeed, given specific knowledge for a particular class of electrode microstructures, the theory can be applied to produce general results. Sensitivity analysis shows that percolation thresholds and TPB lengths depend significantly upon $\bar{Z}$. However, the conductivities generally are weaker functions of $\bar{Z}$. In all cases, the qualitative behavior of the results and the functional forms of the nondimensional properties are independent of a particular $\bar{Z}$.

5.2. Binary mixtures

5.2.1. Percolation thresholds

Percolation thresholds for electrode and electrolyte particles in binary mixtures are predicted by Eqs. (25) and (24). It is evident that these percolation thresholds depend upon the ratio of particle-radii. Fig. 7 shows the relationship between the percolation threshold (represented as electrode volume fractions, ψ^c_{ed}, $1-\psi^c_{\mathrm{el}}$) and the particle-radii ratio $r_{\mathrm{el}}/r_{\mathrm{ed}}$. For a specified $r_{\mathrm{el}}/r_{\mathrm{ed}}$, the volume fraction of electrode particles should be chosen within the range ($\psi^c_{\mathrm{ed}} < \psi_{\mathrm{ed}} < 1-\psi^c_{\mathrm{el}}$), thus assuring that both the electrode and electrolyte particles form connected networks through the entire composite-electrode thickness. Fig. 7 shows that separation between the two curves is greatest near a particle-radii ratio near unity. This means that the acceptable range of electrode volume fractions becomes smaller as the difference in particle-radii increase. It is also evident from Fig. 7 that both curves increase as

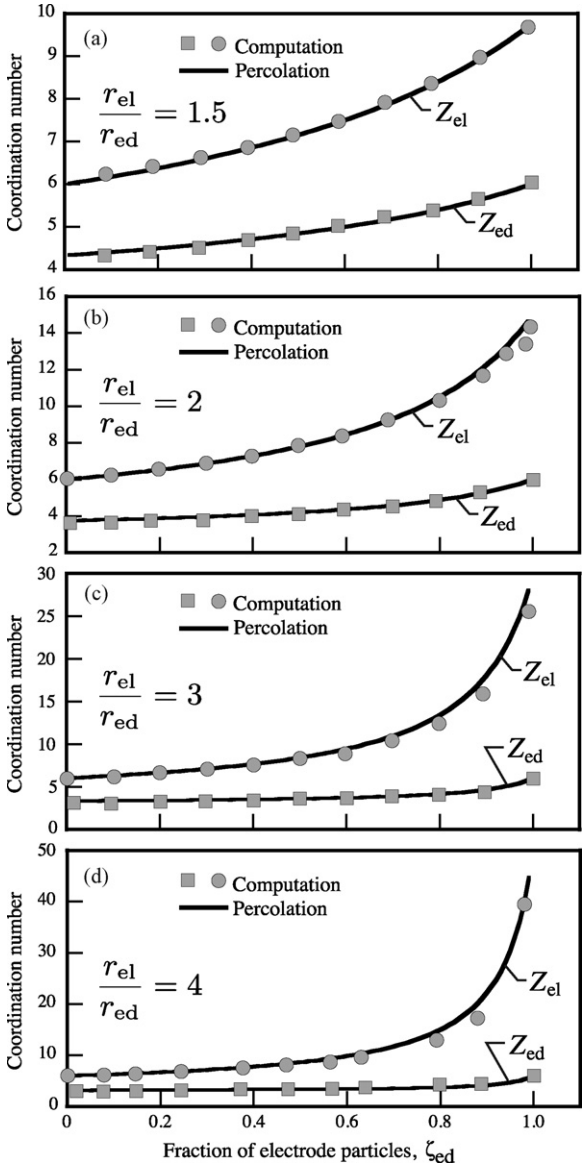

Fig. 6. Comparison of coordination numbers predicted by percolation theory and direct multi-particle computations reported by Suzuki and Oshima [18].

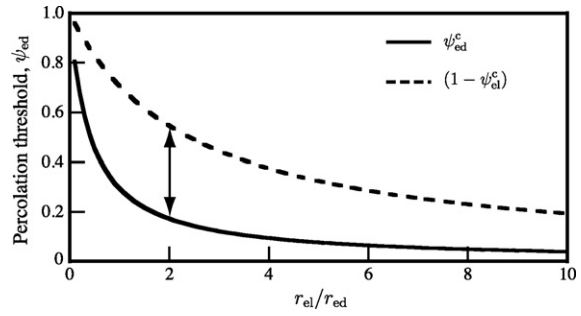

Fig. 7. Percolation thresholds for electrode and electrolyte particles as functions of the particle-radii ratio.

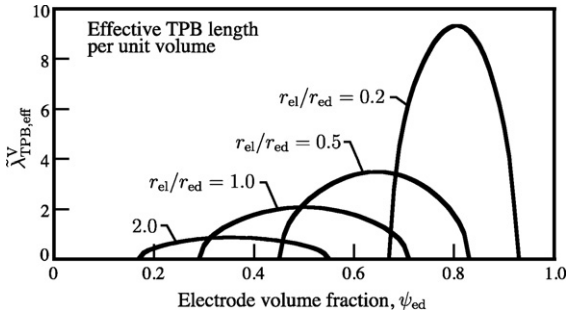

Fig. 8. Nondimensional effective TPB lengths per unit volume as functions of electrode volume loading ψ_{ed} and the particle-radii ratio r_{el}/r_{ed}.

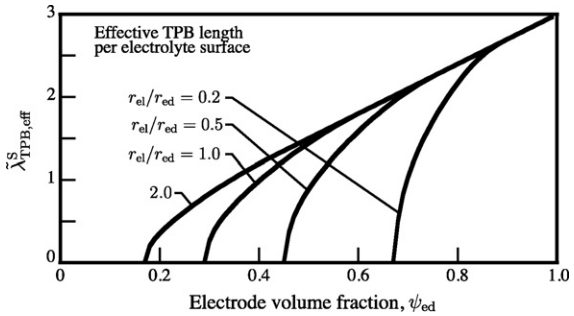

Fig. 9. Nondimensional effective TPB lengths per unit electrolyte surface area as functions of electrode volume loading ψ_{ed} and the particle-radii ratio r_{el}/r_{ed}.

r_{el}/r_{ed} decreases. This means that as the electrode particles become larger relative to the electrolyte particles, increased electrode volume loading is needed to assure complete percolation.

5.2.2. Effective TPB length

Eq. (30) represents the TPB length in a binary mixture. Following substitutions for contact perimeter and particle number loading, the equation can be rewritten as

$$\lambda^{V}_{TPB,eff} = \left[\frac{3}{2}\frac{\min(r_{ed}, r_{el})}{r^3_{ed}}(1-\phi_g)\sin\theta\right]\psi_{ed}Z_{ed,el}P_{ed}P_{el} \quad (51)$$

The effective TPB length depends upon $Z_{ed,el}$, P_{ed} and P_{el}, which are functions of ψ_{ed} and the particle-radii ratio r_{el}/r_{ed}. The TPB length can be written in dimensionless form as

$$\tilde{\lambda}^{V}_{TPB,eff} = \frac{\lambda^{V}_{TPB,eff}}{(1-\phi_g)\sin\theta/r^2_{ed}} \quad (52)$$

The nondimensional effective TPB length per unit volume $\tilde{\lambda}^{V}_{TPB,eff}$ is independent of the particular particle-radii (r_{ed} and r_{el}), and the contact angle θ. However, it does depend upon the particle-radii ratio, the porosity ϕ_g.

Fig. 8 shows how $\tilde{\lambda}^{V}_{TPB,eff}$ depends upon the electrode volume loading ψ_{ed} and the particle-radii ratio r_{el}/r_{ed}. It is evident from the figure that when $r_{el}/r_{ed} = 1$ the maximum $\tilde{\lambda}^{V}_{TPB,eff}$ is at $\psi_{ed} = 0.5$. When $r_{el}/r_{ed} > 1$, the electrode volume loading for the maximum $\tilde{\lambda}^{V}_{TPB,eff}$ decreases. When $r_{el}/r_{ed} < 1$, the electrode volume loading for the maximum $\tilde{\lambda}^{V}_{TPB,eff}$ increases. The shapes of the curves show that $\tilde{\lambda}^{V}_{TPB,eff}$ is only defined within certain threshold limits that depend upon the particle-radii ratio. That is, there are fractional loadings above and below the thresholds for which there is no effective TPB length.

In practical terms, the actual TPB length must be evaluated from the nondimensional function. In this case, values must be assigned for the average contact angle and the porosity. Typical values for the contact angle are around $\theta = 15^{\circ}$ [3,12], but details depend upon the particular composite structure.

The effective TPB length $\lambda^{V}_{TPB,eff}$ affects SOFC performance greatly. The net rate of electrochemical charge-transfer chemistry (i.e., production of useful electric current) depends directly upon the active TPB lengths. Thus, increasing effective TPB length reduces activation overpotential and improves fuel-cell performance.

Although the functional form of the nondimensional $\tilde{\lambda}_{TPB,eff}$ is independent of the particle radius (Eq. (52)), the physical $\lambda_{TPB,eff}$ actually is inversely proportional to the particle sizes. Consider an example in which $r_{ed} = r_{el} = 0.25\,\mu m$ and $\phi_g = 30\%$. Using Fig. 8, it follows that $\lambda^{V}_{TPB,eff} = 6.05 \times 10^{12}\ m/m^3$. However, with $r_{ed} = r_{el} = 50\,nm$, the effective TPB length is increased greatly to $\lambda^{V}_{TPB,eff} = 1.51 \times 10^{14}\ m/m^3$. All other things being equal, this reduction in particle sizes increases current density by a factor of approximately 25. Such behavior is observed experimentally [5–8].

Although usually less important practically, it is also interesting to consider the effective TPB length per unit surface area of the dense electrolyte at its interface with the composite electrode (Eq. (32)). As with the TPB length per unit volume, a nondimensional formulation is helpful; that is

$$\tilde{\lambda}^{S}_{TPB,eff} = \frac{\lambda^{S}_{TPB,eff}}{(1-\phi_g)\sin\theta/r_{ed}}. \quad (53)$$

Fig. 9 shows how $\tilde{\lambda}^{S}_{TPB,eff}$ depends upon the electrode volume loading ψ_{ed} and the particle-radii ratio r_{el}/r_{ed}. As with $\tilde{\lambda}^{V}_{TPB,eff}$ there is a threshold below which there is no effective TPB length per unit surface area. In fact, comparing Figs. 8 and 9 shows that the lower thresholds for ψ_{ed} are the same in both cases. However, there is no upper threshold for $\tilde{\lambda}^{S}_{TPB,eff}$. For a given electrode volume loading fraction (within the threshold), $\tilde{\lambda}^{S}_{TPB,eff}$ generally increases as r_{el}/r_{ed} increases.

5.2.3. Effective conductivity

Fig. 10 shows the effective intra-particle electronic and ionic dimensionless conductivities as functions of electrode volume loading ψ_{ed} and the particle-radii ratio r_{el}/r_{ed}. As in the case of TPB length, there is benefit in representing the results in nondi-

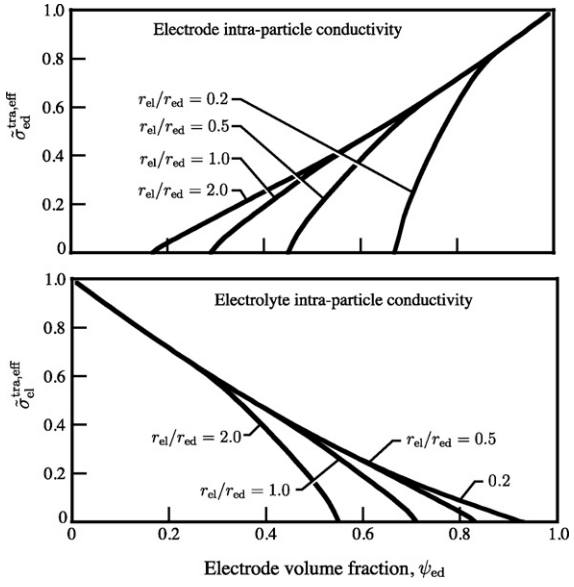

Fig. 10. Nondimensional effective intra-particle conductivity for binary mixtures as functions of electrode volume loading ψ_{ed} and the particle-radii ratio r_{el}/r_{ed}. The upper panel shows the electrode conductivity and the lower panel shows electrolyte conductivity.

mensional terms. In this case, comparison with Eq. (34) indicates the dimensionless form as

$$\tilde{\sigma}_{ed}^{tra,eff} = \frac{\sigma_{ed}^{tra,eff}}{\sigma_{ed}^{tra,o}(1-\phi_g)^{\mu}} = [\psi_{ed}P_{ed}]^{\mu}. \quad (54)$$

An analogous definition is used for the ionic conductivity through the electrolyte particles, $\tilde{\sigma}_{el}^{tra,eff}$.

For a given electrode volume fraction (within the percolation threshold), as the ratio r_{el}/r_{ed} increases, $\tilde{\sigma}_{ed}^{tra,eff}$ increases (Fig. 10a). However, as r_{el}/r_{ed} increases, $\tilde{\sigma}_{el}^{tra,eff}$ decreases (Fig. 10b). At a certain electrode volume loading, electrode conductivity increases as the electrolyte particle radius relative to the electrode-particle radius increases (as long as the particle ratio is within the percolation threshold). However, as the electrode electric conductivity increases as a result of larger electrolyte particles, the ion conductivity decreases. Because of the larger intrinsic conductivity of electrode particles relative to electrolyte particles, the overall conductivity of the composite electrode increases with the increasing electrolyte particle-radii. This behavior is consistent with the results reported by Yu et al. [2].

Fig. 11 shows the dimensionless inter-particle electrode and electrolyte conductivities, which are defined as

$$\tilde{\sigma}_{ed}^{ter,eff} = \frac{\sigma_{ed}^{ter,eff}}{\sigma_{ed}^{ter,o} r_{ed}\sin^2\theta(1-\phi_g)/\delta}, \quad (55)$$

where δ is the thickness of any inter-particle material, such as a grain boundary. For YSZ, grain-boundary thicknesses have been estimated to be around $\delta \approx 5$ nm [33].

Based upon earlier literature, Chan et al. [14] reported specific intra-particle and inter-particle electron resistivities for LSM at 945 °C. The electron conductivities in LSM (nominally the electron conductor) are both around $\sigma_{ed}^{tra,o} = \sigma_{ed}^{ter,o} = 10000$ S/m (specific resistivity around 0.01 Ω cm). As an example consider a situation in which $\psi_{ed} = 50\%$, $r_{el}/r_{ed} = 1$, $r_{ed} = 0.5\,\mu$m, $\phi_g = 0.26$ and $\theta = 15^o$. In this case, based upon the results in Figs. 10 and 11, the effective intra-particle and inter-particle electrode conductivities are $\sigma_{ed}^{tra,eff} = 2126.5$ S/m and $\sigma_{ed}^{ter,eff} = 99440$ S/m. For this material $\sigma_{ed}^{ter,eff} \gg \sigma_{ed}^{tra,eff}$, which means that the inter-particle conductivity

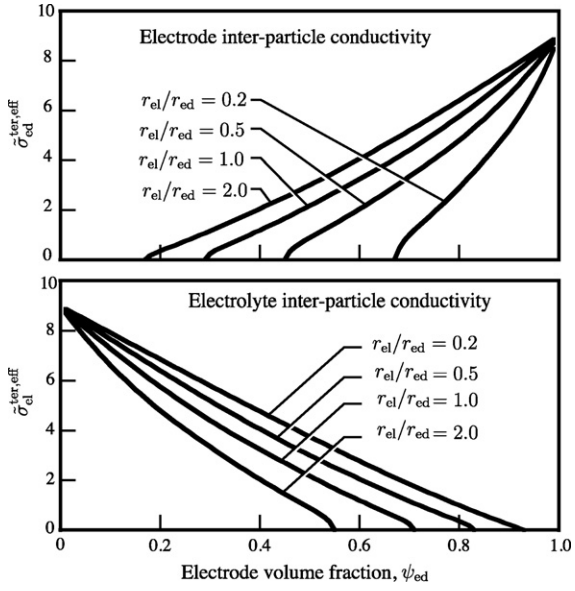

Fig. 11. Nondimensional effective inter-particle conductivity for binary mixtures as functions of electrode volume loading ψ_{ed} and the particle-radii ratio r_{el}/r_{ed}. The upper panel shows the electrode conductivity and the lower panel shows electrolyte conductivity.

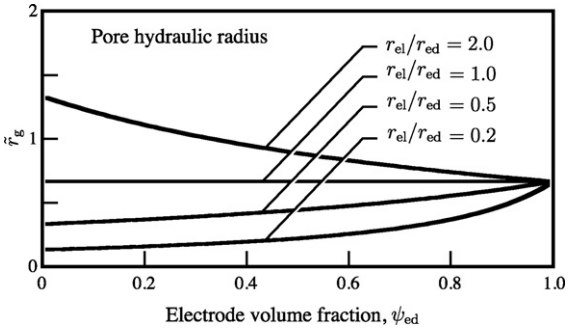

Fig. 12. Nondimensional hydraulic pore-radii as functions of electrode volume loading ψ_{ed} and the particle-radii ratio r_{el}/r_{ed}.

is sufficiently large that it is essentially negligible in offering resistance to electron conduction.

Chan et al. [14] also reported ion resistivities for YSZ at 945 °C. The specific intra-particle and inter-particle ionic conductivities for YSZ are $\sigma_{el}^{tra,o} = 6.7$ S/m (specific resistivity around 15 Ω·cm), and $\sigma_{el}^{ter,o} = 0.05$ S/m (specific resistivity around 2000 Ω·cm). Again consider an example where $\psi_{ed} = 50\%$, $r_{el}/r_{ed} = 1$, $r_{ed} = 0.5\,\mu$m, $\phi_g = 0.26$ and $\theta = 15^o$. Under these circumstances, $\sigma_{el}^{tra,eff} = 1.4$ S/m and $\sigma_{el}^{tra,eff} = 0.5$ S/m. In this case, both intra- and inter-particle conductivity contribute significantly to the net ion conduction.

5.2.4. Pore hydraulic radius

The pore radius can be an important parameter in the controlling gas transport within the porous electrode structure. Fig. 12 is a nondimensional representation of pore radius as a function of electrode volume fraction and particle-radii ratio. The dimensionless radius is defined as

$$\tilde{r}_g = \frac{r_g}{r_{ed}/(1-\phi_g)}. \quad (56)$$

For $r_{el}/r_{ed} = 1.0$, $\tilde{r}_g$ is independent of the electrode volume fraction. For relatively larger electrode particles (i.e., $r_{el}/r_{ed} < 0.5$, the dimensionless pore radius increases as ψ_{ed} increases. For relatively smaller electrode particles (i.e., $r_{el}/r_{ed} > 0.5$, the dimensionless pore radius decreases as ψ_{ed} increases. For a certain ψ_{ed}, $\tilde{r}_g$ increases as the electrolyte-particle radius increases relative to the electrode-particle radius.

5.3. Three-component mixtures

This section considers a three-component mixture, comprised of a single type of electron-conducting particle (labeled ed) and two sizes of ion-conducting particles (labeled el_1 and el_2). Such an electrode configuration is motivated by Itoh et al., who found that composite Ni-YSZ electrodes with both coarse and fine YSZ particles prevented the agglomeration of Ni and improved long-term cell performance [34].

5.3.1. Percolation thresholds

Eq. (44) involves four parameters for three-component mixtures: r_{ed}/r_{el_1}, r_{el_2}/r_{el_1}, ψ_{ed}, and $\psi_{el_2}^o$). Fig. 13 shows the percolation regions as functions of r_{el_2}/r_{el_1} and $\psi_{el_2}^o$, but with the ratio r_{ed}/r_{el_1} fixed at unity. The regions between the upper dashed curve and the lower solid curve (i.e., values of the percolating electrode-particle volume fraction) are the regions in which both the electrode and electrolyte particles form connected networks throughout the entire thickness of the composite-electrode structure. High-performance electrode structures are usually designed to be within this fully percolated region.

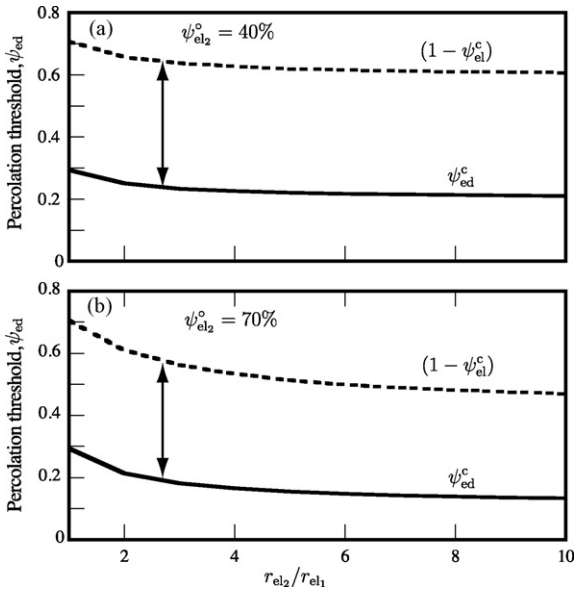

Fig. 13. Percolation thresholds ψ^{c}_{ed} and $(1-\psi^{c}_{el})$ in a three-component mixture as functions of r_{el_2}/r_{el_1}, and $\psi^{o}_{el_2}$, with $r_{ed}/r_{el_1} = 1$.

The region between ψ^{c}_{ed} and $(1-\psi^{c}_{el})$ decreases as r_{el_2}/r_{el_1} increases at fixed volume fraction of the larger electrolyte particles $\psi^{o}_{el_2}$. There is a relatively weak, but still significant, influence of the volume loading of the larger electrolyte particles $\psi^{o}_{el_2}$ (i.e., compare Fig. 13 a and 13b). Beyond $r_{el_2}/r_{el_1} > 10$ the percolation thresholds become essentially independent of the particle-size ratio.

5.3.2. Effective TPB length

By restricting Eq. (45) to a three-component mixture (one size electrode particle r_{ed}, and two sizes of electrolyte particles, r_{el_1} and r_{el_2}), the equation can be rewritten as

$$\lambda^{V}_{TPB,eff} = \frac{3}{2}(1-\phi_g)\psi_{ed}\sin\theta \times \left(\frac{\min(r_{ed}, r_{el_1})}{r^3_{ed}} Z_{ed,el_1} P_{ed} P_{el} + \frac{\min(r_{ed}, r_{el_2})}{r^3_{ed}} Z_{ed,el_2} P_{ed} P_{el} \right). \quad (57)$$

In this equation $Z_{k,\ell}$, P_{ed} and P_{el} are functions of each component's volume fraction and the particle-radii ratios r_ℓ/r_k. Because both sizes of electrolyte particles are connected to form the network (i.e., a percolated A cluster), it may be assumed that $P_{el_1} = P_{el_2}$. Thus, a single probability P_{el} appears in Eq. (57), and its value can be estimated using Eqs. (23) and (43). The effective TPB per unit volume is put into nondimensional form as

$$\tilde{\lambda}^{V}_{TPB,eff} = \frac{\lambda^{V}_{TPB,eff}}{(1-\phi_g)\sin\theta/r^2_{ed}}. \quad (58)$$

Fig. 14 shows the nondimensional effective TPB lengths per unit volume as functions of electrode particle volume loading, electrolyte–particle-radii ratio, and the large-radius electrolyte volume loading. In all cases, the electrode-particle radius is the same as the small electrolyte-particle radius (i.e., $r_{ed}/r_{el_1} = 1$). The boundaries of the percolation thresholds are evident in Fig. 14. Outside these thresholds, where the particles are not fully percolated, any TPB length is ineffective. It is also evident from the figure that as the size and the volume fraction of larger electrolyte particles increase, the electrode volume fraction ψ_{ed} for the maximum nondimensional TPB length decreases.

Fig. 15 shows nondimensional effective TPB lengths per unit surface area of dense electrolyte in a three-component mixture. The

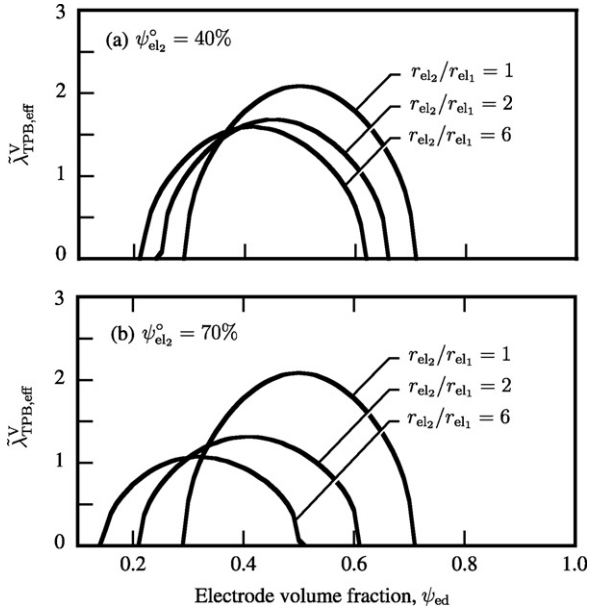

Fig. 14. Nondimensional effective TPB lengths per unit volume in a three-component mixture as functions of electrode volume fraction ψ_{ed}, r_{el_2}/r_{el_1}, and $\psi^{o}_{el_2}$, with $r_{ed}/r_{el_1} = 1$.

nondimensional function is formed as

$$\tilde{\lambda}^{S}_{TPB,eff} = \frac{\lambda^{S}_{TPB,eff}}{(1-\phi_g)\sin\theta/r_{ed}}. \quad (59)$$

The nondimensional surface-based TPB length increases monotonically as the electrode volume fraction increases. At relatively low electrode volume loading, the surface-based TPB length increases as the radius of the larger electrolyte increases (i.e., r_{el_2}/r_{el_1} increases). For large electrode volume loading (i.e., $\psi_{ed} > 0.5$), the surface-based TPB length becomes essentially independent of the electrolyte size distribution.

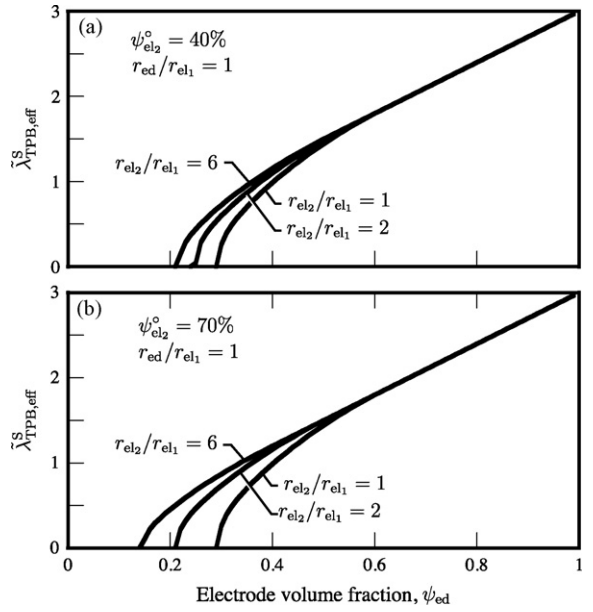

Fig. 15. Nondimensional effective TPB lengths per unit surface area of dense electrolyte in a three-component mixture as functions of electrode volume fraction ψ_{ed}, r_{el_2}/r_{el_1}, and $\psi^{o}_{el_2}$, with $r_{ed}/r_{el_1} = 1$.

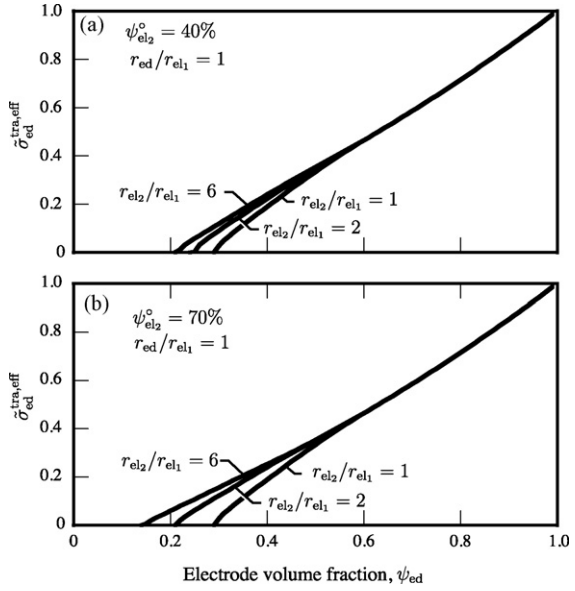

Fig. 16. Nondimensional effective intra-particle electrode conductivities in a three-component mixture as functions of electrode volume fraction ψ_{ed}, r_{el_2}/r_{el_1}, and $\psi^{o}_{el_2}$, with $r_{ed}/r_{el_1} = 1$.

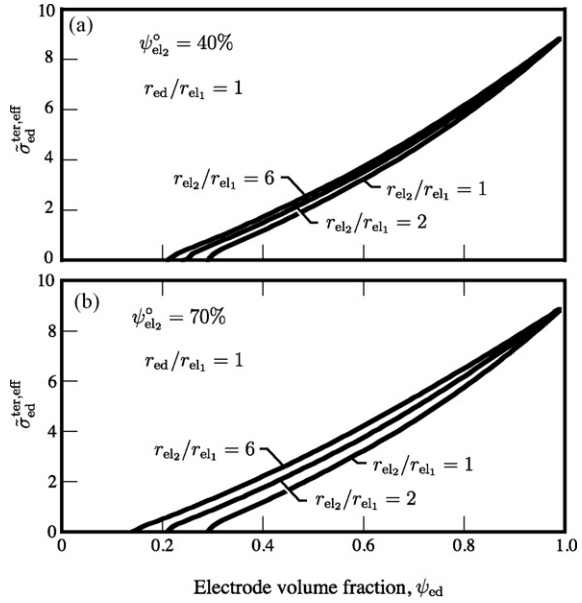

Fig. 18. Nondimensional effective inter-particle electrode conductivities in a three-component mixture as functions of electrode volume fraction ψ_{ed}, r_{el_2}/r_{el_1}, and $\psi^{o}_{el_2}$, with $r_{ed}/r_{el_1} = 1$.

5.3.3. Effective conductivities

Figs. 16 and 17 show the nondimensional intra-particle electrode and electrolyte conductivities in a three-component mixture as functions of electrode volume fraction ψ_{ed}, r_{el_2}/r_{el_1}, and $\psi^{o}_{el_2}$. In all cases, the electrode-particle radius is the same as the smaller electrolyte-particle radius (i.e., $r_{ed}/r_{el_1} = 1$). Qualitatively the behavior is similar to situation for binary mixtures. Electrode conductivity increases monotonically as the electrode volume fraction increases. For low electrode-particle loading the nondimensional intra-particle electrode conductivity increases with increasing radius of the larger electrolyte particles. However, for $\psi_{ed} > 0.5$, the intra-particle conductivity becomes essentially independent of the relative sizes of the electrolyte particles. The nondimensional electrolyte intra-particle conductivity decreases monotonically as the electrode volume fraction increases. For low electrode volume fraction, the electrolyte intra-particle conductivity become essentially independent of the electrolyte-particle size ratio (Fig. 17).

Figs. 18 and 19 show the nondimensional inter-particle electrode and electrolyte conductivities in a three-component mixture as functions of electrode volume fraction ψ_{ed}, r_{el_2}/r_{el_1}, and $\psi^{o}_{el_2}$. In all cases, the electrode-particle radius is the same as the smaller electrolyte-particle radius (i.e., $r_{ed}/r_{el_1} = 1$). Qualitatively the behavior is similar to the situation for the inter-particle conductivity in binary mixtures. That is, the inter-particle electrode conductivity increases and the electrolyte conductivity decreases with increasing electrode volume loading. Because of its functional

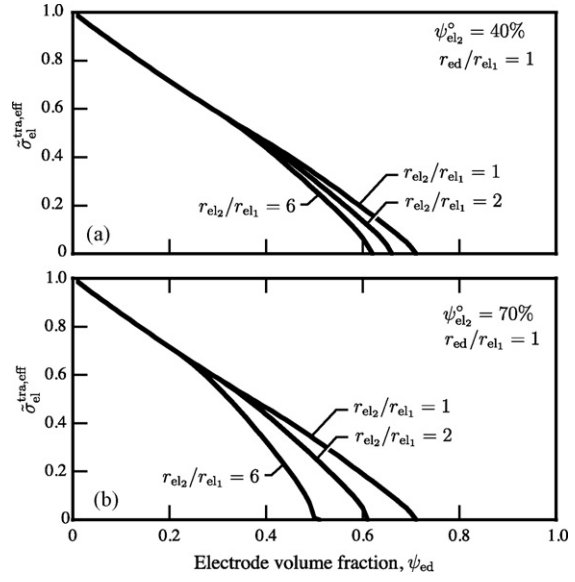

Fig. 17. Nondimensional effective intra-particle electrolyte conductivities in a three-component mixture as functions of electrode volume fraction ψ_{ed}, r_{el_2}/r_{el_1}, and $\psi^{o}_{el_2}$, with $r_{ed}/r_{el_1} = 1$.

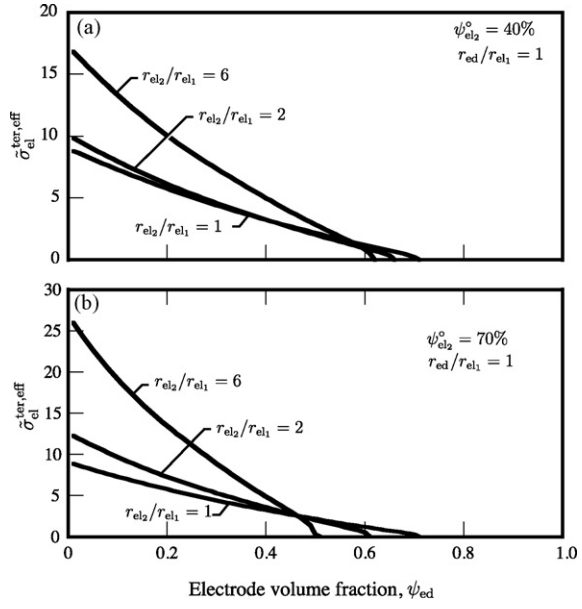

Fig. 19. Nondimensional effective inter-particle electrolyte conductivities in a three-component mixture as functions of electrode volume fraction ψ_{ed}, r_{el_2}/r_{el_1}, and $\psi^{o}_{el_2}$, with $r_{ed}/r_{el_1} = 1$.

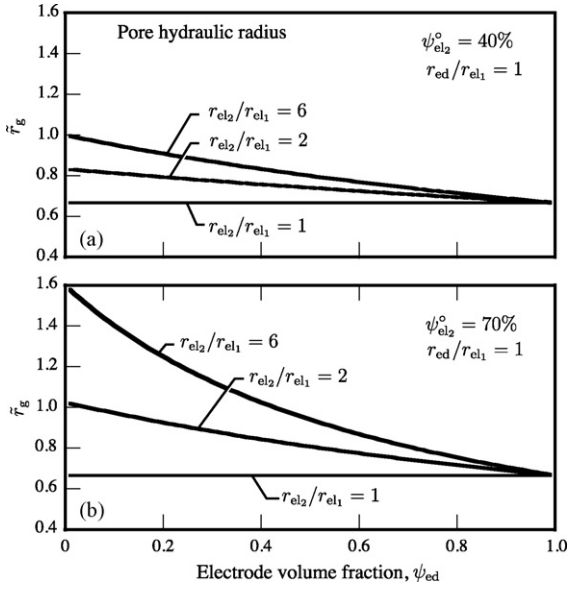

Fig. 20. Nondimensional hydraulic pore radius in a three-component mixture as functions of electrode volume fraction ψ_{ed}, r_{el_2}/r_{el_1}, and $\psi^{o}_{el_2}$, with $r_{ed}/r_{el_1} = 1$.

form, the nondimensional inter-particle conductivity $\tilde{\sigma}^{ter,eff}$ is independent of the particle radius (Eq. (55)). However, the physical inter-particle conductivity $\sigma^{ter,eff}$ (i.e., in dimensional form) will increase with the increasing of particle sizes.

5.3.4. Pore hydraulic radius

Fig. 20 shows the nondimensional hydraulic pore radius in a three-component mixture. The nondimensional pore radius is defined as

$$\tilde{r}_g = \frac{r_g}{r_{ed}/(1-\phi_g)}. \quad (60)$$

The ratio of electrolyte particle sizes has a strong influence upon the pore radius, especially at relatively low electrode volume loading. The pore radius increases significantly as the larger electrolyte particle size increases.

6. Summary and conclusions

A percolation theory model is developed to predict effective properties in SOFC composite electrodes. Such properties, including ion and electron conductivities, three-phase boundary lengths, and hydraulic pore radii, are needed to assist optimizing electrode structures and for inclusion into larger scale models that use effective properties in continuum-based models. The models accommodate binary and multi-component mixtures of ion- and electron-conducting particles. The effective properties for an entire electrode structure depend upon physical characteristics, including particle size, packing density, intrinsic material properties, and porosity. Thus the models provide a quantitative connection between measurable and controllable characteristics at the particle scale with overall performance at the composite-electrode scale. All the results are presented in nondimensional form, which increases generality for application of the model.

Acknowledgements

We gratefully acknowledge the financial support of the Knowledge Innovation Program and the Key Program of the Chinese Academy of Sciences (KJCX1.YW.07), the National High-Tech R&D Program of China (2007AA05Z156) and the National Science Foundation of China (10574114). The effort at the Colorado School of Mines was supported by the US Office of Naval Research through a Research Tools Consortium (N00014-05-1-0339).

References

[1] F. Zhao, A.V. Virkar, J. Power Sources 141 (2005) 79–95.
[2] J.H. Yu, G.W. Park, S. Lee, S.K. Woo, J. Power Sources 163 (2007) 926–932.
[3] D.H. Jeon, J.H. Nam, C.J. Kim, J. Electrochem. Soc. 153 (2) (2006) A406–A417.
[4] M. Shah, J.D. Nicholas, S.A. Barnett, Electrochem. Commun. 11 (2008) 1–4.
[5] Z. Jiang, L. Zhang, K. Feng, C. Xia, J. Power Sources 185 (2008) 40–48.
[6] J. Chen, F. Liang, L. Liu, S.P. Jiang, B. Chi, J. Pu, J. Li, J. Power Sources 183 (2008) 586–589.
[7] S. Kim, H. Moon, S. Hyun, J. Moon, J. Kim, H. Lee, J. Power Sources 163 (2006) 392–397.
[8] J. Yoon, R. Araujo, N. Grunbaum, L. Baque, A. Serquis, A. Caneiro, X. Zhang, H. Wang, Appl. Surf. Sci. 254 (2007) 266–269.
[9] J.R. Wilson, W. Kobsiriphat, R. Mendoza, H.Y. Chen, J.M. Hiller, D.J. Miller, K. Thornton, P.W. Voorhees, S.B. Adler, S.A. Barnett, Nat. Mater. 5 (2006) 541–544.
[10] H. Zhu, R.J. Kee, V.M. Janardhanan, O. Deutschmann, D.G. Goodwin, J. Electrochem. Soc. 152 (2005) A2427–A2440.
[11] H. Zhu, R.J. Kee, J. Electrochem. Soc. 155 (7) (2008) B715–B729.
[12] P. Costamagna, P. Costa, V. Antonucci, Electrochim. Acta 43 (1998) 375–394.
[13] P. Costamagna, M. Panizza, G. Cerisola, A. Barbucci, Electrochim. Acta 47 (2002) 1079–1089.
[14] S.H. Chan, X.J. Chen, K.A. Khor, J. Electrochem. Soc. 151 (2004) A164–A172.
[15] X.J. Chen, K.A. Khor, S.H. Chan, L.G. Yu, Mater. Sci. Eng. A335 (2002) 246–252.
[16] V.M. Janardhanan, V. Heuveline, O. Deutschmann, J. Power Sources 178 (2008) 368–372.
[17] D. Bouvard, F.F. Lange, Acta Metall. Mater. 39 (1991) 3083–3090.
[18] M. Suzuki, T. Oshima, Powder Technol. 35 (1983) 159–166.
[19] M. Suzuki, T. Oshima, Powder Technol. 44 (1985) 213–218.
[20] M. Suzuki, T. Oshima, Powder Technol. 43 (1985) 19–25.
[21] S. Sunde, J. Electrochem. Soc. 143 (1996) 1930–1939.
[22] L.C.R. Schneider, C.L. Martin, Y. Bultel, L. Dessemond, D. Bouvard, Electrochim. Acta 52 (2007) 3190–3198.
[23] J. Deseure, Y. Bultel, L.C.R. Schneider, L. Dessemond, C.L. Martin, J. Electrochem. Soc. 154 (2007) B1012–B1016.
[24] A. Ali, X. Wen, K. Nandakumar, K.T. Chuang, J. Power Sources 185 (2008) 961–966.
[25] J. Golbert, C.S. Adjiman, N.P. Brandon, Ind. Eng. Chem. Res. 47 (2008) 7693–7699.
[26] C.H. Kuo, P.K. Gupta, Acta Metall. Mater. 43 (1995) 397–403.
[27] T. Saito, Y. Akiyama, N. Ishida, T. Yasuo, S. Taniguchi, S. Murakami, N. Furukawa, Denki Kagaku 61 (1993) 228–233.
[28] T. Kawada, N. Sakai, H. Yokokawa, M. Dokiya, M. Mon, T. Iwata, J. Electrochem. Soc. 137 (1990) 3042–3047.
[29] T. Kawada, N. Sakai, H. Yokokawa, M. Dokiya, M. Mon, T. Iwata, Solid State Ionics 40–1 (1990) 402–406.
[30] M.J. Verkerk, B.J. Middelhuis, A.J. Burggraaf, Solid State Ionics 6 (1982) 159–170.
[31] L.C.R. Schneider, C.L. Martin, Y. Bultel, D. Bouvard, E. Siebert, Electrochim. Acta 52 (2006) 314–324.
[32] J.H. Nam, D.H. Jeon, Electrochim. Acta 51 (2006) 3446–3460.
[33] M.J. Verkerk, B.J. Middelhuis, A.J. Burggraaf, Solid State Ionics 6 (1982) 159–170.
[34] H. Itoh, T. Yamamoto, M. Mori, J. Electrochem. Soc. 144 (1997) 641–646.